National Weather Service
Office of Meteorology

Technical Procedures Bulletin

Subject: Changes to the 1998 NCEP Operational MRF Model Analysis/Forecast System

Series No. 449

Science Division, Silver Spring, MD 20910

ABSTRACT

An extensive package of changes will be made to the NCEP global analysis and forecast system on 15 June 1998 at 1200 UTC. The changes include (1) An increase in horizontal and vertical resolution from T126l28 to T170L42 for the analysis and first 84 forecast hours; (2) physics updates, affecting radiation and clouds, land surface parameterization, cumulus convection and gravity wave drag; (3) analysis and data assimilation updates, including changes in time interpolation, nonlinear interpolation, limits on supersaturation and negative moisture, background error covariance, 3-D ozone, level 1-b polar orbiter data, GOES radiances, and Y2K compliance. During the first two months in which the new package was run in parallel with the operational, the following features were observed: (1) reduction in the wet bias in precipitation over land (Fig. 5.6b); (2) reduction of the cold bias over much of the atmosphere, including the stratosphere and near-surface layers, together with the appearance of a warm bias over land in the lower atmosphere, all reflecting changes in the surface physics and in the radiation, and (3) improvement in the model's ability to maintain transient eddy kinetic energy throughout the forecast (Fig. 5.2a) and (Fig. 5.2b). The objective performance statistics for 1-2 months of testing show clear improvement in precipitation bias, reduction in jet-level rms vector error versus analysis - especially in the short range - (Fig. 5.3), increased accuracy of tropical winds versus analysis (Fig. 5.4), and no significant change in 5-day 500-hPa anomaly correlations for geopotential (Fig. 5.5).

LeRoy Spayd
Chief, Training and Professional
Development Core

Changes to the 1998 NCEP Operational MRF Model Analysis/Forecast System:

John Derber, Hua-Lu Pan, Jordan Alpert, Peter Caplan, Glenn White, Mark Iredell, Yu-Tai Hou, Ken Campana and Shrinivas Moorthi

National Centers for Environmental Prediction

W/NP23, World Weather Building,
Washington DC 20233, USA

ABSTRACT

An extensive package of changes will be made to the NCEP global analysis and forecast system on 15 June 1998 at 1200 UTC. The changes include (1) An increase in horizontal and vertical resolution from T126l28 to T170L42 for the analysis and first 84 forecast hours; (2) physics updates, affecting radiation and clouds, land surface parameterization, cumulus convection and gravity wave drag; (3) analysis and data assimilation updates, including changes in time interpolation, nonlinear interpolation, limits on supersaturation and negative moisture, background error covariance, 3-D ozone, level 1-b polar orbiter data, GOES radiances, and Y2K compliance. During the first two months in which the new package was run in parallel with the operational, the following features were observed: (1) reduction in the wet bias in precipitation over land (Fig. 5.6b); (2) reduction of the cold bias over much of the atmosphere, including the stratosphere and near-surface layers, together with the appearance of a warm bias over land in the lower atmosphere, all reflecting changes in the surface physics and in the radiation, and (3) improvement in the model's ability to maintain transient eddy kinetic energy throughout the forecast (Fig. 5.2a) and (Fig. 5.2b). The objective performance statistics for 1-2 months of testing show clear improvement in precipitation bias, reduction in jet-level rms vector error versus analysis - especially in the short range - (Fig. 5.3), increased accuracy of tropical winds versus analysis (Fig. 5.4), and no significant change in 5-day 500-hPa anomaly correlations for geopotential (Fig. 5.5).

1.0 INTRODUCTION

On 15 June 1998 changes to the following areas in the MRF analysis/forecast system will be implemented:

Resolution, increased from T126 to T170 in the horizontal and L28 to L42 in the vertical

Physics, including changes in:

- Land surface package
- Cumulus convection
- Gravity wave drag
- Radiation and clouds
- 3-D ozone

Analysis and data assimilation, including changes affecting:

- Time interpolation
- Nonlinear interpolation
- Limits on supersaturation and negative moisture
- Background error covariance
- 3-D ozone
- Level 1-b data from polar orbiter
- GOES radiances
- Y2K compliance

In this Technical Procedures Bulletin, for the sake of clarity the model that is to be replaced will be referred to as the "old" or "operational" model, while the new model will be referred to in the present tense, even though the TPB was posted before the implementation.

2.0 RESOLUTION INCREASE (M. Iredell)

Because small-scale features in the atmosphere tend to be more transient than the larger-scale features, it was expected that increased resolution in the global model would most benefit the short-term forecasts and in particular the data assimilation system. Therefore, both horizontal and vertical resolution have been increased in the global model to T170 L42 for the Final global data assimilation system, the full 4-per-day 78-hour Aviation forecasts and the first 84 hours of the Medium Range Forecast (MRF). (An exception is in the rare case when a forecast must be run on the backup computer, in which case it would be run in degraded resolution.) The MRF (beyond forecast hour 84) as well as the other ensemble members remain unchanged in resolution from the previous configuration. All the T170 L42 forecasts are run with the new prognostic ozone; all the T126 L28 and T62 L28 forecasts are run with climatological ozone. A summary of the different resolutions for all the global model forecasts can be found in Table 1.

The horizontal resolution has been increased to global spectral triangular truncation T170 from T126. Thus the wavelength of the shortest resolvable wave on the globe has been reduced to just over 2 degrees from almost 3 degrees, which is roughly equivalent to increasing the grid resolution to 80 km from 105 km.

The model nonlinear dynamics is computed on an alias-free 512 by 256 Gaussian dynamics grid. However, the interpolation to observations in the analysis and the physics parameterizations in the model are computed on the same 384 by 190 Gaussian physics grid as previously. This physics grid will resolve any feature in the T170 spectral model, since it still has significantly higher resolution than its so-called linear grid resolution of 340 by 170. Both the orography and the diabatic physics terms in the spectral model are lightly filtered near the end of the spectrum (up to a 40% reduction at wavenumber 170) in order to reduce the direct forcing of the shortest waves. This filter follows Lander and Hoskins (1997), which suggested that the shortest waves in a spectral model be reserved purely for nonlinear dynamical forcing. The model post-processing grid remains an equidistant 360 by 181 cylindrical grid. The isobaric fields on this grid are filtered at around wave number 120 compared to wave number 90 in the previous model.

Fig. 2.1 shows model orography over the eastern U.S. for the T170 resolution and the T126 resolution. Note that the higher resolution now allows a finer characterization of the White Mountains in New Hampshire and the Great Smokies on the border between Tennessee and North Carolina. Also note that the 10-meter Gibbs rolls in the Atlantic Ocean have been greatly reduced. A general reduction of Gibbs phenomena in the orographic forcing and in the physics forcing is due to both higher resolution and the light filter of orography.

The vertical resolution has been increased to 42 sigma levels from 28 sigma levels. The extra resolution is fairly evenly distributed in the atmosphere, with about 3 new levels in the stratosphere, about 8 new levels in the middle to upper troposphere and about 3 new levels in the boundary layer. In the jet region around 250 hPa, the vertical resolution is now less than 1.0 km where in the previous implementation it was greater than 1.5 km. It is anticipated that this increase in resolution should help to improve both the accuracy and the sharpness of jet wind forecasts for aviation purposes. The top sigma level is now around 2.0 hPa, up from the 2.7 hPa top level in the previous 28-layer model. The vertical distribution of levels is now minimally adequate to simulate prognostic ozone in the stratosphere.

The new vertical distribution of 42 sigma levels is shown in Fig. 2.2 Note that the distribution of levels is smoothly varying in the vertical. This is necessary in order to minimize the truncation error in vertical differentiation and integration. Furthermore, there is an emphasis on resolution in the boundary layer, in order to provide greater characterization of inversions and fronts as well as to minimize vertical truncation error. Although the vertical resolution is fine in the stratosphere when viewed in the pressure coordinate, it resolution is quite coarse in the height coordinate, the appropriate coordinate for stratospheric dynamics.

The change of resolution for the MRF at hour 84 (to T126 L28) and hour 168 (to T62 L28) is accomplished with minimal impact on the forecast. A digital filter initialization is run in the new lower resolution with the added cost of 3 forecast integration hours in order to reduce the transient noise caused by any imbalances resulting from the change of resolution.

Several steps have been taken to fit the higher-resolution model into the available time windows on the computer. First, several data processing steps have been better optimized. The SSM/I and ERS-2 surface winds processing has been moved earlier in the cycle in order to minimize the delays caused by these steps. The SSI analysis has been greatly optimized to multiprocess its work across the whole computer. The spectral model also is better spread over the computer. The cost of a quadratic model physics grid had been found to be much greater than its benefit, so its relative grid size has been reduced as mentioned above. The T170 L42 SSI analysis now takes about 15 minutes on the Cray C916 and the T170 L42 global spectral model takes about 15 minutes per forecast day.

References:Lander, J. and B.J.Hoskins, 1997: Believable Scales and Parameterizations in a Spectral Transform Model, *Mon. Wea. Rev.*, **125**, 292-303.

3.0 CHANGES TO THE OPERATIONAL FORECAST MODEL

3.1 Land-surface parameterization upgrades (H.-L.Pan)

- Additional climatological dataset: Formerly we used 0.7 for vegetation cover globally; we now use a monthly mean vegetation cover, based on an NDVI (Normalized Difference Vegetation Index) climatology.

- Other additional datasets: soil type and vegetation type database. We now have eight soil categories and eleven vegetation categories. This is the database used in the current eta model.

- Canopy water: Maximum canopy water content has been reduced from 2 mm to 0.5 mm. Tests have shown that 2 mm takes too long to evaporate and leads to air temperature forecast errors. The new value is taken from the eta model.

- Transpiration: The transpiration formulation has been modified to include resistance due to PAR (Photosynthetically Active Radiation), air humidity and air temperature. Transpiration did not cease after dark in the current MRF formulation, but the use of PAR will allow for it. Furthermore, the additional resistance allows for a decrease of transpiration when air becomes too hot or too dry. The new formulation follows that of the current eta model.

- Snow cover: Partial snow cover is now allowed in a grid box when the snow depth is less than one inch. This is a very first step in recognition of the fact that partial snow cover is very important in the temperature forecast.

- Frozen soil: A frozen soil condition is now allowed, so that runoff can be properly simulated when the soil is frozen.

- Snow depth: The snow depth estimate from the snow cover analysis is now reduced. Operationally, we used a minimum of 25 mm of water equivalent snow depth in our estimate. In view of tests that showed that it takes too long to melt this amount, this has now been changed to 5 mm. We hope to get a global snow depth analysis by next winter.

- Runoff: The surface runoff has been increased. The previous formula called for runoff only after the topsoil is saturated. We have modified it to start runoff when 15% of the grid box becomes saturated. This parameterization is in accord with the local nature of precipitation.

- Roughness length: Thermal roughness length is now allowed to be different from momentum roughness length. The thermal roughness formulation over the ocean based on TOGA observations is now extended to the land. This allows for a larger skin-to-air temperature gradient which is more realistic, according to FIFE comparison studies.

3.2 Convection changes (H.-L.Pan)
The model uses a Simplified Arakawa-Schubert scheme with the quasi-equilibrium closure:

$$M_b = (A - \text{alpha}(w)\, A_c) / \text{tau}(w)$$

where A is the cloud work function, A_c is a critical cloud work function that is cloud-depth dependent, w is the vertical motion, alpha and tau are tuned parameters based on cloud bottom large-scale vertical motion, and M_b is the mass flux that will provide the balance between grid scale and the cloud scale environment. We have now modified alpha to reduce the critical cloud work function to allow for earlier initiation of convection when the cloud base vertical motion is upward. We also modified the upper limit of alpha to change the scheme to a CAPE elimination scheme with a lower value of omega. This is done only over the ocean to reduce the precipitation bulls-eye problem encountered during the summer of 1997.

In addition to the above changes, a modification of the evaporation formulation for convective rain has also been made. The current MRF model has a strong tendency to dry out the regions of convection, leading to a negative bias in the precipitable water field. This was suspected in 1995 when the model was run for a time with SSM/I precipitable water data and a marked spin-down in relative humidity resulted. Since observations show that significant evaoration occurs when the environmental shear is strong, we have modified the evaporation efficiency factor from a constant value of .07 to a factor that depends on wind shear, following Fritsch and Chappell (1980). This change has led to significant improvement in the global humidity climatology of the model. This change was made only over ocean grid points.
References:Fritsch, J. M. and C. F. Chappell, 1980: Numerical Prediction of convectively-driven mesoscale pressure systems. Part I: Convective parameterizaion, *J. Atmos. Sci.*, **37**, 1722-1733.

3.3 Enhanced gravity wave drag (and improved modeled leeside mountain cyclogensis(Jordan Alpert, Song-You Hong [General Sciences Corporation] and Young-Joon Kim [UCLA])

Gravity wave drag arises from the interaction of sub-grid scale gravity waves generated by the wind and orography and the subsequent vertical propagation of these waves and their interaction with the atmospheric momentum in the lower and upper troposphere. The model response to GWD is to warm the "too-cold" polar regions, improve the too-low height bias, and improve jet stream and cyclone track positions in large spatial scales and climate of the model - a general improvement to NWP model systematic errors. However, the modeled treatment of GWD parameterization in the lower troposphere is lacking in a number of respects. Improvements to the operational GWD are from two new orographic files in addition to the orography variance, $(h')^2$:

1.Orographic asymmetry designed for determining the drag enhancement associated with low level wave breaking,

2.Orographic convexity designed to incorporate the effects of multiple irregular barriers.

3.The gravity wave stress includes sensitivity to the direction of the wind impinging on the face of the mountains (In the old scheme, only one variance for one face of the mountains was used).

The tropospheric enhancement of low-level wave-breaking is from a scheme based on the work of Kim(1995) and has been applied to the MRF model. A case study of the February, 1995 "Valentine's day" storm, known for strong leeside mountain cyclogenesis and a cold air outbreak, reveals the potential effects of a weakly-acting phenomenon such as GWD. The GWD enhancement showed improved modeled storm intensity and position of the cyclone for this particular case. A short description of this case follows. A verifying mean sea level pressure (MSLP) analysis shown in Fig. 3.1 for 15 Feb 1990 0000 UTC can be compared with 36-h model forecasts verifying at this time. The storm is now well defined and located in northern Colorado with the maximum pressure gradient to the north of the storm center. The operational MRF control 36-h forecast in Fig. 3.2 shows the storm at least 4 hPa too deep and displaced about 200-300 km to the northeast into Nebraska. The forecast with enhanced GWD is shown in Fig. 3.3 . where the storm center motion is retarded about halfway between the operational MRF in Fig. 3.2 and the observed position in Fig. 3.1. The lowest closed contour is the same as that for the operational run, 988 hPa, but the areal extent for the enhanced GWD is smaller than the operational model's, indicating a slightly less intense storm.

There is evidence that NWP models often fail in predicting the correct intensity of leeside mountain cyclogenesis and the often accompanying movement of cold air outbreaks. Indeed, the model treatment of small-scale boundary layer friction drag and the interaction with the variance in orography is still known incompletely in NWP models. The GWD parameterization, while weakly-acting, influences the cyclone track speed and development intensity by removing small-scale biases as well as continuing to reduce large-scale biases, benefiting the model, by reducing mid-latitude westerlies and warming the polar atmosphere.

References:Kim, Y.-J., 1995: Improvement of orographic gravity wave parameterization using a mesoscale gravity wave model. *J. Atmos. Sci*,**52**, 1875-1902.

3.4 Radiation and clouds (Y.-T. Hou and K. Campana)

The NCEP operational shortwave (SW) radiation parameterization was developed at the Geophysical Fluid Dynamics Laboratory, using portions of the scheme from Lacis and Hansen (JAS, 1974, p118). While the longwave (LW) parameterization has been upgraded several times in the past ten years, the SW method has not changed. A newer, more accurate, method has been developed at NCEP, based on the work of NASA's Chou and Lee (JAS, 1996, p1204, as well as Chou, JAS, 1992, p762). The new SW scheme consists of a multi-spectral band technique, an improved calculation in cloudy atmospheres, the addition of climatological aerosol effects, and a new surface albedo, which is a function of 14 distinct surface types.

Monthly forecast experiments with a T62 model, using the changes to the SW scheme, showed significant improvement to the model-computed radiation budget (Table 1), at both the top of the atmosphere (TOA) and earth's surface (SFC). Improvements in the surface albedo can be seen for the July 1985 test in Fig. 3.4, where the control (CNTL) contains the currently operational SW algorithm, the experimental (EXP) contains the new SW scheme, and the observed (ERBE) is derived from TOA flux data. The operational model overestimates global planetary albedo, while it is significantly reduced to more realistic values in the new scheme. Atmospheric SW radiative heating is enhanced in the new model, resulting in a warmer troposphere, especially in the tropics (generally 0.5 - 1.0 degree K in the zonal averages). Computational overhead with the new SW scheme is less than 5%.

TABLE 1 Global SW Radiation Budget (W/m2)
(data at earth's surface estimated from satellite measurements)

	MONTH	OBSERVED	NEW SW	OPNL SW
TOA-upward	JUL 85	98.0	97.1	105.4
	JAN 86	109.5	108.0	117.8
TOA-up clear	JUL 85	51.5	49.6	50.3
	JAN 86	56.1	53.8	55.7
Net at SFC	JUL 85	151.6	158.5	160.7
	JAN 86	159.0	166.9	168.7

Concurrent with the change to the SW parameterization, the LW scheme is slightly modified in regions of model multi-layer cloud. In the operational model, radiative heating rates within these multi-layer clouds are adjusted to the same value for all cloud layers, that is, there is no large LW cooling at the cloud top, as is observed in the atmosphere. This 'LW adjustment' is a leftover from an earlier NCEP era, when zonal mean cloud was persisted during a global forecast. Large values of continuous cloud top cooling within the persisted clouds was found to be detrimental to the forecast, and the heating rate adjustment was found to ameliorate the problem. Additionally, the adjustment was consistent with the procedure used in the old SW scheme. Since the new SW scheme has removed this feature, the LW algorithm has thus been made consistent with it.

The diagnostic cloud formulation is used only in the radiation calculations (Campana etal, 1994, *10th AMS Conference on NWP*). The operational model diagnoses cloud coverage from model temperature and moisture, in the form of relative humidity, throughout the model troposphere. A set of cloud/humidity relationships was developed from daily mean US Air Force RTNEPH cloud analyses during August 1993-February 1994. Clouds in the lowest 10% of the atmosphere are allowed only in suspected marine stratus regions (*i.e.* oceanic moist inversion, capped by very dry air). Consequently, especially over land, low stratus is not well modeled, with occasional detrimental effects on near-surface (sensible) weather. The scheme has now been retuned to more recent synoptic (not daily mean) RTNEPH data (March-December 1995) and modified to include cloud/humidity relationships for lower atmospheric clouds everywhere over the globe. Fig. 3.5, shows an example of the improvement to modeled low stratus cloud over the eastern US in the new scheme. The top portion of the figure contains the average lower atmosphere cloud fractional coverage during hours 18-21 of a T126L28 global forecast, where the old (left) and new (right) schemes are shown for a case in January 1995. The bottom of the figure shows the US AirForce observations for that time (the missing values in the observations result from data that are too old for the 18-21 hour forecast or where low cloud is obscured by higher cloud (satellite observations over the oceans). The cloudiness being advected down the northeast and middle Atlantic coast appears better modeled in the new scheme.

When all the new components of the forecast model are included in the T170 model, the improvements to radiation and cloud parameters are quite striking. During the 10-day period, 14-23 March 1998, global planetary albedo values dropped from 35.6% to 32.6%, downward SW radiation at the earth's surface dropped by 15 W/m2, and total cloud cover increased from 47% to 53% for the new model. All changes are in the correct sense. Fig. 3.6, shows the mean of the daily 12-36 hour total cloud cover forecast for the 14-23 March 1998 period, for the new model, operational model, and RTNEPH analyses. The new clouds appear superior to the operational T126L28 data when compared with the mean of the RTNEPH analyses over this period.

3.5 Prognostic Ozone (S. Moorthi and M. Iredell)

Ozone is generated through photochemical processes above ~ 25 km from the earth's surface and carried to the stratosphere and upper troposphere through advection and mixing. The vertical profile of ozone generally has significant values above an altitude of 8 km with a peak value

around an 10 to 30 km. Its strong absorption of solar ultraviolet radiation, is the dominant heat source in the stratosphere and is very important to the stratospheric general circulation. Ozone also plays an important role in the infrared radiative transfer in the stratosphere. Thus, accurate prediction of ozone is important to both numerical weather prediction as well as long-term climate predictions and global change studies.

The previous operational MRF model at used a very crude representation of ozone by prescribing a zonal and seasonal mean climatology. This assumption was especially inaccurate for long-range and climate prediction. Furthermore, a reliable first guess of ozone is now necessary for an accurate forward model from model space to radiance space for the assimilation of TOVS- and GOES-measured radiances. Thus including ozone as a prognostic variable will help the assimilation/forecast system in two ways. First, by providing more accurate radiative heating of the atmosphere, it can provide improved first guess fields for the analyses. Secondly, the predicted ozone itself is a necessary first guess field in the direct assimilation of radiances. Also, accurate prediction of spatial variability of ozone can help in improving the prediction of UV index (which gives a measure of harmful ultra-violet radiation reaching the earth's surface), thus improving our ability to warn the public.

	The new model includes ozone as a three-dimensional prognostic variable. The continuity equation for ozone can be written as

$$dX/dt = P - LX + X_d$$

where X is the ozone mixing ratio in kg/kg, d/dt is the material derivative, P is the photochemical production rate (source), L is the destruction rate per unit ozone mixing ratio (sink), and X_d is weak horizontal and vertical diffusion of ozone. The ozone advection is treated exactly in the same manner as that for specific humidity, with Eulerian spectral approach. The source and sink terms are parameterized based on the zonal average, ten-day mean climatological data obtained from the GSFC two-dimensional model (R. Rood, A. Douglas, and M. Cerniglia, personal communication). The continuity equation is solved by time splitting. First, a provisional value of X is obtained after applying horizontal and vertical advection. Then the diffusion is applied in an implicit manner, the horizontal diffusion in spectral space and the vertical diffusion in grid-point space. Finally, the photochemical effects are applied, photochemical destruction being treated implicitly (Rood et al., 1991). Inclusion of prognostic ozone adds about 10% to the CPU time of the model.

An example of a typical ozone forecast is given in Fig. 3.7a and Fig. 3.7b where the forecasts are in the top row and the verifying analyses in the bottom row.

References:

Rood, R., A. R. Douglas, J. A. Kaye, M. A. Geller, C. Y. Chen, D. J. Allen, E. M. Larsen, E. R. Nash, J. E. Nielsen, 1991: Three-dimensional simulations of wintertime ozone variability in the lower stratosphere. *J. Gephys. Res*., **96** , # D3, 5055-5071.

4.0 CHANGES TO THE ANALYSIS SYSTEM [(J. C. Derber, W.-S. Wu (GSC), R. Treadon (GSC), T. Matsumura (JMA) and B. Katz (GSC)]

4.1 Improved time interpolation.

In the previous version of the analysis, the 6-hour forecast, used as a background (first guess), was interpolated between the zero and 6-hr forecast to the observation time if it was prior to the

analysis time. If the observation time fell after the analysis time, the 6-hr forecast was used at the observation time.

Since the development of the previous version of the analysis, the 3 and 9 hr forecasts have become available to the analysis. Since all observations fall between the 3 and 9 hr forecast times, it is now possible to linearly interpolate to all observation times with the largest interpolation being 1.5 hours. This change resulted in small reductions in the fit of the observations to the background, with the largest changes (but still small) being for satellite radiances. In most cases the impact of this change should be small, with the largest changes for small scale rapidly moving systems.

4.2 Nonlinear analysis

The new SSI analysis system has been modified in two ways to incorporated nonlinearities in the analysis. First, the minimization algorithm has been changed to be a nonlinear minimization algorithm. At this time, the only nonlinear components in the minimization are the SSM/I wind speeds and in the limitation on the negative and supersaturated moisture described below. For the SSM/I wind speeds, the introduction of the nonlinear minimization algorithm allows the use of the wind speed data without the creation of a direction. In the previous version of the analysis system, the wind direction was created using a local analysis of the wind direction. Since the SSM/I winds were often located far from any conventional data, the created wind direction often reflected the background wind direction. This resulted in the background wind direction being given too much weight and the near surface wind analysis was slightly degraded. The most significant impact of this change was in the southern hemisphere where a slight positive impact was noted.

The second change that introduces nonlinearities is the external iteration. The external iteration is a loop around the entire analysis procedure which allows the inclusion of weak nonlinearities in the observation and balance constraints which would be too expensive to include directly in the minimization algorithm. For example, the radiance calculation for the moisture channels is nonlinear. However, the nonlinearity is weak enough that it can be included by relinearizing around the solution every so often. Experiments indicate that the nonlinearities included in the external iteration could be well accounted for by relinearizing about 5 times. However, the computational expense of the external iteration is currently too large to perform 5 external iterations. Therefore in the current implementation there are only 2 external iterations (i.e., calculated observational increments, linearize, perform 37 minimization iterations and then repeat). This is not ideal, but allows a significant enhancement in the inclusion of nonlinearities in the analysis system and has allowed a significant increase in the weight given the moisture channels for the satellite radiances.

4.3 Limiting supersaturation and negative moisture.

In the previous version of the analysis, the supersaturation and negative values were limited only at the end of the analysis. The limitation on the supersaturation and negative values was such that it could not exceed supersaturation or become negative except if the guess was

supersaturated or negative. In this case, the values were limited by the guess values. This formulation of the limitation on the supersaturation and negative moisture was allowing areas of negative moisture to grow in the analysis and not properly distributing integrated moisture quantities (i.e., total precipitable water, satellite radiances) properly in the vertical.

In the new version of the analysis, the inclusion of the nonlinearities in the analysis allows a direct penalization of supersaturated and negative values in the minimization. Since the constraint is not exact, it does allow negative and supersaturated values (which is necessary for the grid to spectral transformation), but it makes it much more unlikely to get supersaturated or negative values. This change should make persistent negative areas unlikely in the analysis and will allow the projection of integrated moisture information more properly in the vertical.

4.4 Reformulated background error covariance.

A new formulation for the background error covariance, which determines the spatial and multivariate distribution of information in the analysis, has been incorporated in the SSI analysis system. This formulation is similar to that documented in Derber and Bouttier (1998) and Bouttier et al. (1997) and applied in the ECMWF forecast model. The new formulation allows a specification of a spatial variance field, reformulates the balance equation, and defines the spectral statistics as a function of total wave number. This reformulation allows much greater flexibility and should result in future improvements to the analysis system. In the current implementation of the new formulation, the spatial variance fields are only allowed to vary by lattitude. In future implementations, this field will vary with the synoptic situation and include information on the presence of hurricanes. The major impact of the new background error covariance is to improve the tropical analyses and forecasts and to better model the lattitudinal variation in the moisture field.

4.5 3-D ozone.

Previously, the ozone analysis was a 2-D total ozone analysis performed separately from the temperature, moisture and wind analysis. A 3-D ozone analysis has become desirable in order to use radiances in the ozone analysis and to include predicted ozone in the forecast model. Also, it has became desirable to combine the analyses together. There is little impact on the thermodynamic variables except through the radiance forward operator, but greatly simplifies the analysis code. Because of the 3-D nature of the ozone analysis, it was necessary to include ozone profile information. SBUV data was made available on an orbit-by-orbit basis and this data has been incorporated in the ozone analysis. Note, because of this change, radiances from the polar orbiters and the geostationary satellites are directly influencing the ozone analysis and NESDIS total ozone retrievals are no longer being used. The ozone analysis suffers from a lack of data and a lack of a long history of improvements. While the basic features of the analysis and forecast are reasonable, the ozone analysis should not yet be considered mature. Evaluation of the new 3-D ozone analyses and forecasts are ongoing with Climate Prediction Center and future significant improvements to the ozone analysis can be expected.

4.6 Changes in the use of polar orbiting level 1-b data.
Several changes to the use of the polar orbiting data have been made. The changes can be divided into two catagorize; changes in the input data set, and changes to the radiative transfer calculations. The changes to the input data set have primarily involved the inclusion of additional satellite data. First, the radiances from NOAA-11 (both HIRS and MSU) have been incorporated into the analysis. The inclusion of this data with that from the NOAA-12 MSU and the NOAA-14 HIRS and MSU means that data from 3 different polar orbiting satellites are currently being used in the analysis system. In addition, less thinning of the MSU and the HIRS data have been done, resulting in additional satellite data being used for all satellites.

The radiative transfer used for the satellite data has undergone extensive changes. The transmittance calculation in the radiative transfer has been changed to a version from NESDIS called OPTRAN (McMillin et al., 1995). Substantial changes to the OPTRAN and the radiative transfer code was necessary to reduce computational cost, to allow the use of different satellites and to remove coding errors. The surface emissivity calculations have also been modified for both the microwave and the infrared channels. For the microwave channels, the effects of surface polarization have been included for each channel and a frequency dependence has been introduced in the surface emissivity. For the infrared, a simple model for the surface emissivity as a function of satellite zenith angle, frequency and wind speed based on Masuda et al. (1988) has been included. The effects of the infrared emissivity model are more important for the geostationary radiances discussed below because of the larger scan angles, but they do have a nontrivial impact also for the polar orbiting data.

4.7 Inclusion of GOES radiances.
With the inclusion of the OPTRAN transmittance calculation, it became possible to directly use radiances from GOES-8 and GOES-9 over the oceanic regions. The radiances used are supplied by NESDIS operations and are only available where NESDIS has determined there are clear fields of view. Several quality control checks were introduced into the analysis. Most importantly, the ability to simulate channel 8 within 1^0C is used to eliminate those field of views that are slightly cloud or land contaminated. For this check, the inclusion of the surface emissivity calculation mentioned in the previous section was particularly important. Also any profile which is created from less than 3 field of views (of a 5x5 block) has been eliminated. Other quality control procedures similar to those used in the polar orbiting data are also applied. A bias correction similar to the bias correction used for the polar orbiting data has also been included (McNally et al., 1998 previous tpb ref.). The observational errors assigned to the GOES radiances are similar to those from the polar orbiting data. Only data which is observed within +/- 1.5 hrs of the analysis time are used. The primary impact of this data appears to be on the moisture fields over the Eastern Pacific and the Western Atlantic.

4.8 T170 42 levels.
With the increase in model resolution, the analysis resolution was also increased. The increased resolution has two primary effects on the analysis. First the better resolution of the orography decreases the differences between the observed and modeled elevation and improves the

resolution of local orographic effects. Because of this, the simulated observations from the background field will fit the observations better. The improved vertical resolution primarily impacts the satellite radiances resulting in improved forward calculations for the radiances.

4.9 Y2K compliance

The analysis system was modified to the fullest extent possible to be Y2K compliant. The only component not yet Y2K compliant is the reading of the BUFR input data set containing the conventional observations since the file is not yet converted to Y2K format. This final conversion will occur soon.

References:

Bouttier, F., J. Derber, and M. Fisher, 1997: The 1997 revision of the J_b term in 3D/4D-var. ECMWF Research Department Tech. Memo. No. 238, available from ECMWF, Shinfield Park, Reading RG29AX, UK..

Derber, J. and Bouttier F., 1998: A reformulation of the background error covariance in the ECMWF global data assimilation system. Submitted to Tellus.

McNally, A. P., J.C. Derber W.-S. Wu, B.B. Katz, 1998:Previous TPB

Masuda, K. T. Takshima and Y. Takayama, 1988: Emissivity of pure and sea waters for the model sea surface in the infrared window regions. Remote Sens. Environ., 24, 313-329.

McMillin, L. M., L. J. Crone, and T.J. Kleespies, 1995: Atmospheric transmittance of an obsorbing gas. 5. Improvements to the OPTRAN approach. Applied Optics, 34, 8396-8399.

5. PARALLEL TESTING AND EVALUATION (G.H. White and P. Caplan)

The new implementation reduces several biases in the global forecasts. Fig. 5.1 shows the temperature bias in 5-day forecasts by the operational and new models each verified against its own system's analyses for a two-week period in late March and early April. The new model substantially reduces a cold bias in the tropical and midlatitude tropopause, although it has somewhat more warm bias in the polar regions in the tropopause and more cold bias in the stratosphere. The reduced cold bias in much of the atmosphere reflects greater diabatic heating due to the new radiation and soil physics. The new model's cloudiness also appears in better agreement with independent estimates of cloudiness from satellite observations, although oceanic regions of low-level stratus now appear to have too little cloudiness. The new system also has warmer low-level temperatures over land, correcting a cold bias in the operational system.

One longstanding problem in the operational model has been a tendency for the forecasts to show less variability than the the analyses. The problem is illustrated in Fig. 5.2a, which shows the zonal mean transient eddy kinetic energy at 250 mb in five-day forecasts and verifying analyses for a two-week period in late March and early April. This is the energy associated with daily deviations from the two-week mean. Five-day forecasts with the operational model show subtantially less day-to-day variability at nearly all latitudes than the verifying analyses. Five-day forecasts with the new model display nearly the same variability as the verifying analyses as can be seen in Fig. 5.2b.

Over the period in which the new analysis/forecast system was run daily in parallel the objective scores (each model vs. its own analysis) showed clear improvement in the rms vector errors in the jet-level winds over North America and the Northern Hemisphere, especially in the first few days of the forecasts Fig. 5.3. The winds in the tropics showed substantial improvement Fig. 5.4. The 500-mb anomaly correlations for geopotential in the extratropics were essentially the same for the new and old models, as shown in Fig. 5.5. Evaluation of precipitation forecasts w done over the first 12-36 hour period in the form of threat and bias scores over the U.S. Improvement in the former can be seen, especially in the light amounts, while the bias is considerably better for all amounts, as shown in Fig. 5.6a and Fig. 5.6b. A useful extension of this threat and bias technique of evaluating precipitation forecasts can be obtained by directly applying it to windspeeds. This was done for 24-h forecasts of 200-hPa winds, with the results shown in Fig. 5.7a and Fig. 5.7b for four regions. Of particular interest for aviation are N. America and the Northern Hemisphere where for all windspeeds out to 60 m/sec the threat score in the new model(T170) is better than in the old (MRF). For the bias, the improvement is especially striking: on the order of half of the negative bias of the windspeed is removed. For example, for wind speeds over 50 m/sec over N. America, the MRF had a bias of .83, meaning that the area enclosed by the 50 m/sec isotach was too small by 17%. In the T170, the bias was about 0.92, too small by 8%. A limited sample of evaluations of model winds and temperatures against rawinsonde and aircraft observations was available. The results (not shown) confirmed the findings of a low-level warm bias over land, but also showed a reduced the operational cold bias in the tropical lower troposphere. The negative wind speed bias was largely removed in the upper troposphere, but at the price of some increase in the rms vector wind errors there, a result inconsistent with the verifications against analyses shown above in Fig. 5.3. This disagreement will be the subject of future research.

6.0 CHANGES IN MODEL OUTPUT FORMAT

For information about file changes go to

http://www.ncep.noaa.gov/NCO/PMB/announcements/t170chngs.html

7.0 SUMMARY

An extensive package of changes has been implemented in the MRF/GDAS system, including increases in the horizontal and vertical resolution, and improvements in the physics, data assimilation and analysis. The new model produces less precipitation over the U.S., substantially reducing the old model's wet bias. Improvements were also noted in precipitation

threat scores here and in evaluations of tropical winds at 200 and 850 hPa and in the winds at 200 hPa in the extratropics when verified against analyses. The new model atmosphere was better able to maintain its transient eddy kinetic energy, but there was some apparent loss of skill of upper tropospheric winds where verified against observations. The new model is warmer in most areas correcting the old model's cold bias (however, the bias is overcorrected and a warm bias introduced in the lower atmosphere over land). For tropical disturbances, the new model damps out much of the low-level noise present in the old model, but only partially eliminates the problem of the generation of spurious disturbances.

8.0 LOOKING AHEAD

Due to constraints on computer resources, it was not possible to run two T170 systems in parallel for complete tuning of the large package of changes described in this TPB. When the installation and testing of a new Class 8 computer are complete early in 1999, we will be able to tune the new system more thoroughly. Our plans for the immediate future include:

- Monitoring and subsequent improvement of known model deficiencies, including: (a)the warm bias in low levels of the model, primarily over land surfaces, (b) slight increases in rms vector wind errors verified against observations and (c) the persistence of some tendency to produce spurious tropical systems. Experiments will be performed to determine causes and to suggest cures. Though several changes in both this and recent implementations were made to address the tropical problem, the higher resolution may exaggerate this tendency.

- Continuation of efforts to improve precipitation forecasts (noted in TPB 443 Nov, 1997): The number of data sources will increase as NOAA-15 data become available, thus enhancing the model's initial conditions; the effort to use satellite-based cloud and precipitation in the analysis will continue; development will continue on the improvement of precipitation products using data from global ensembles; experimentation with prognostic cloud water will continue with the creation of an initial analysis of cloud water linked to the convection and radiation parameterizations.

- Testing of improved usage of GOES winds and scatterometer data.

- Improved initialization, with special attention to the tropics.

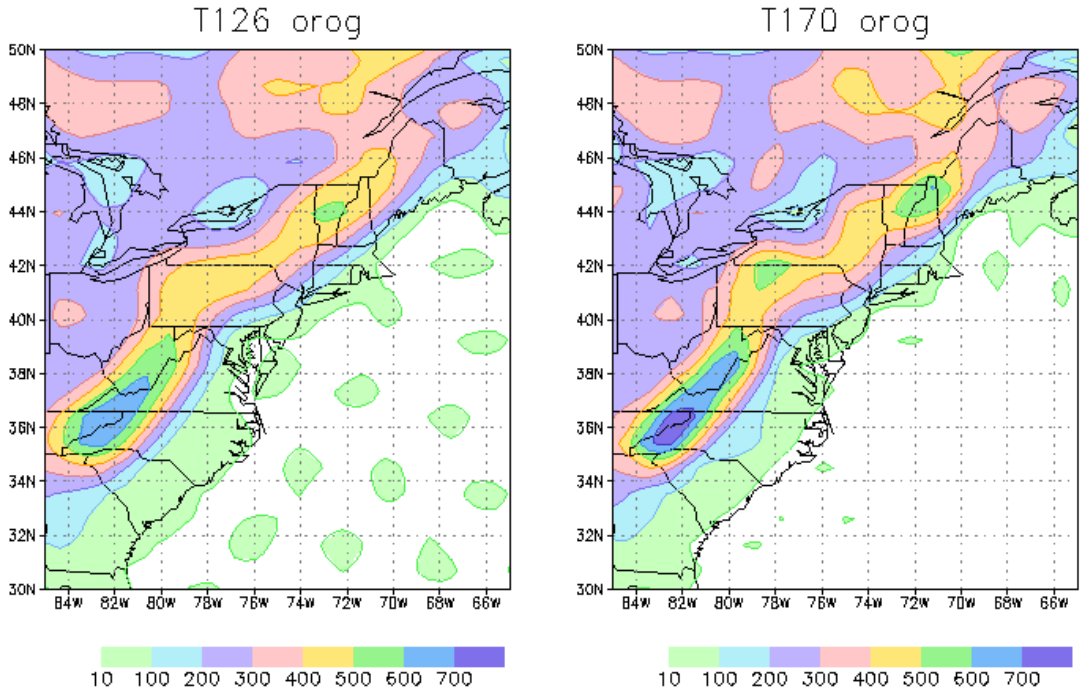

Fig. 2.1 Orography (m) for T126 (left) and T170 (right).

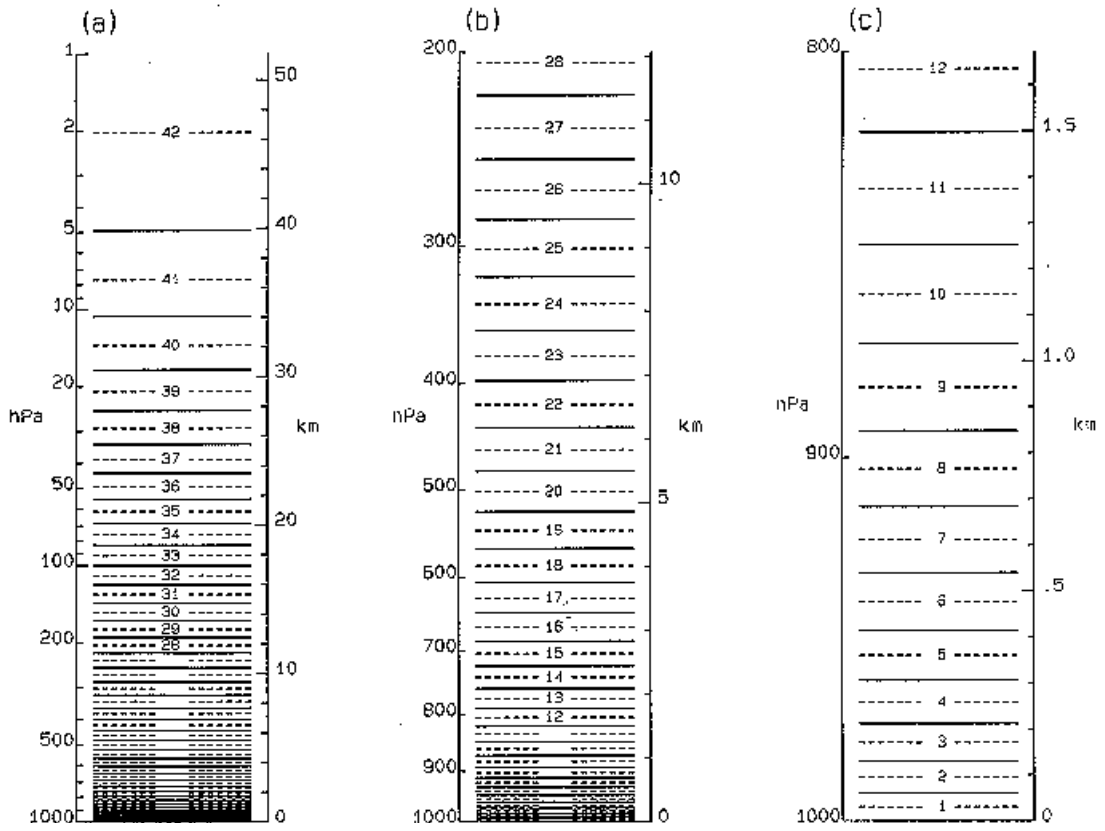

Fig. 2.2 Spacing of the 42 model sigma layers as a function of height and pressure for the entire atmosphere(left)
, 1000-200 hPa (center) and 1000-800 hPa (right).

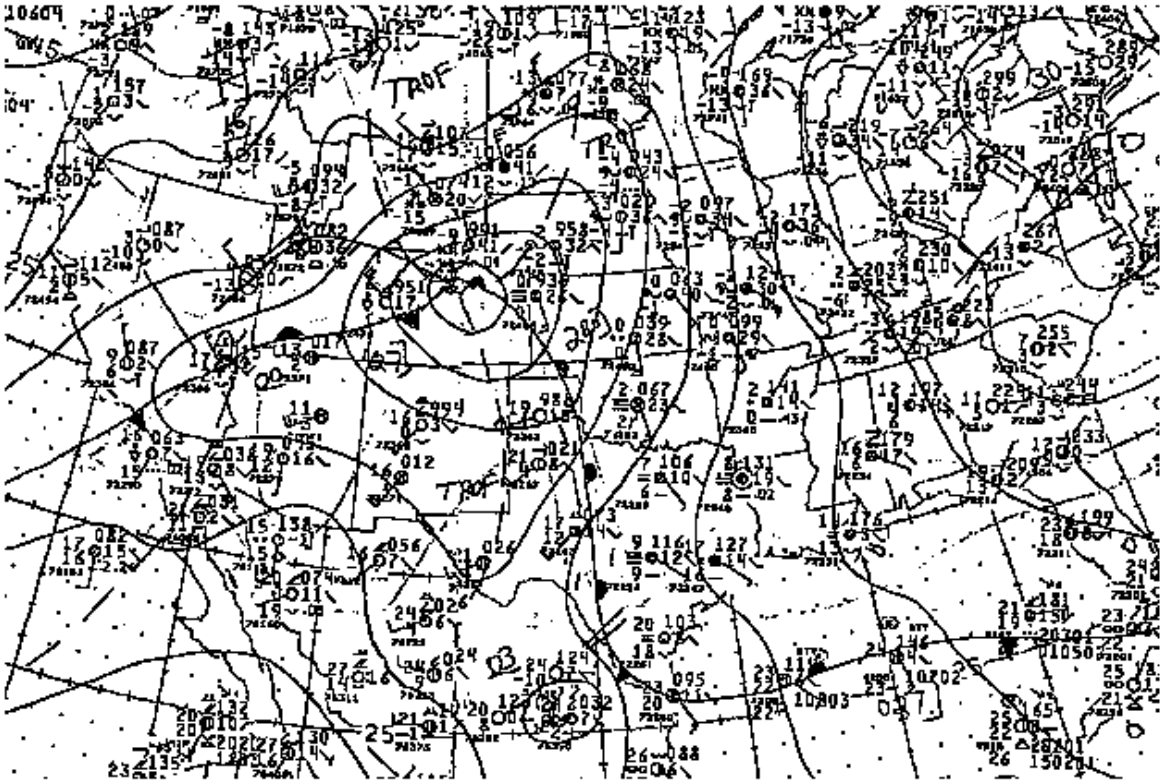

Figure 1. EMC global analysis of Mean Sea Level Pressure 15FEB95 00Z

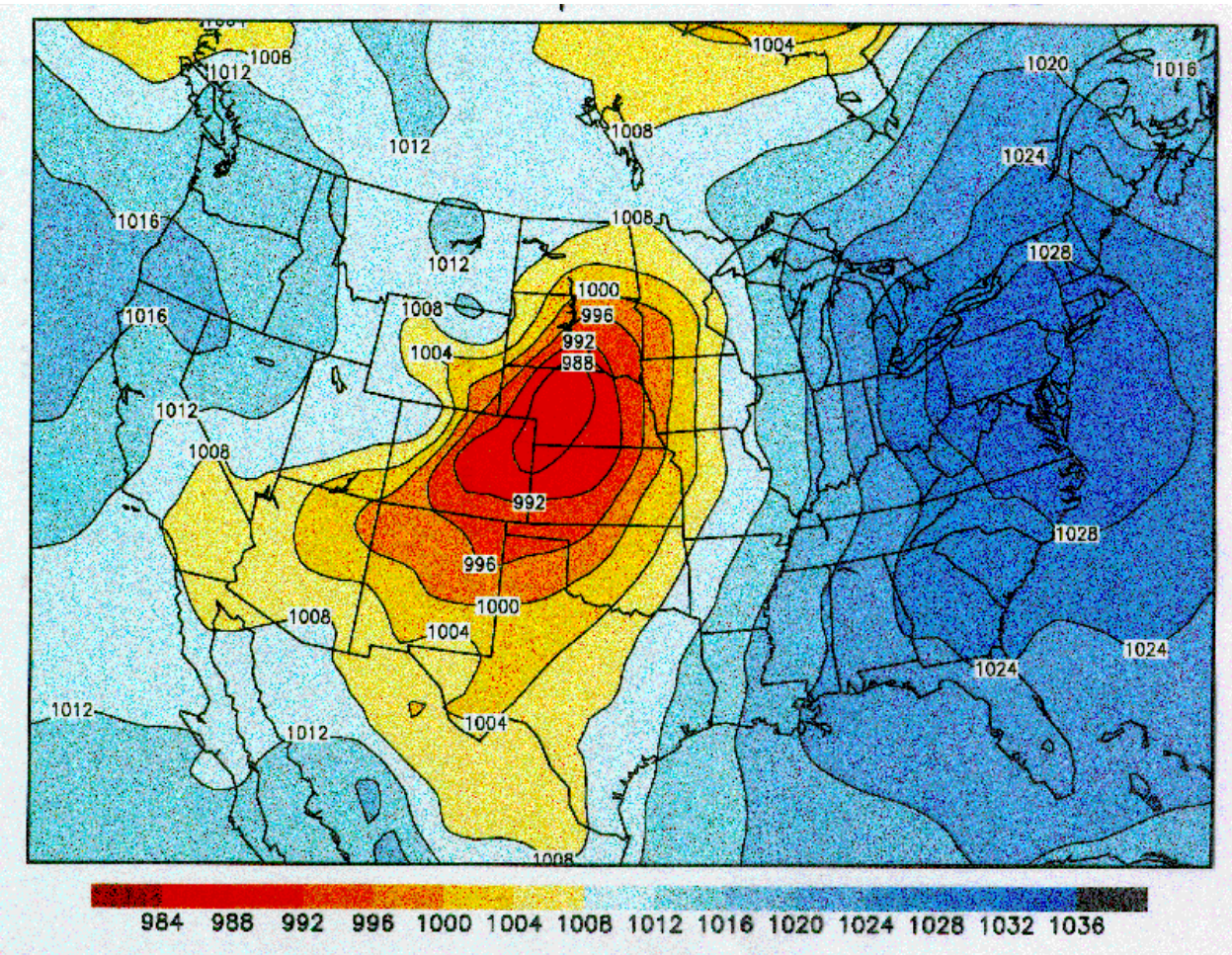

Fig. 3.2 Operational 36-h MRF forecast of mean sea-level pressure valid 0000 UTC 15 Feb 1998.

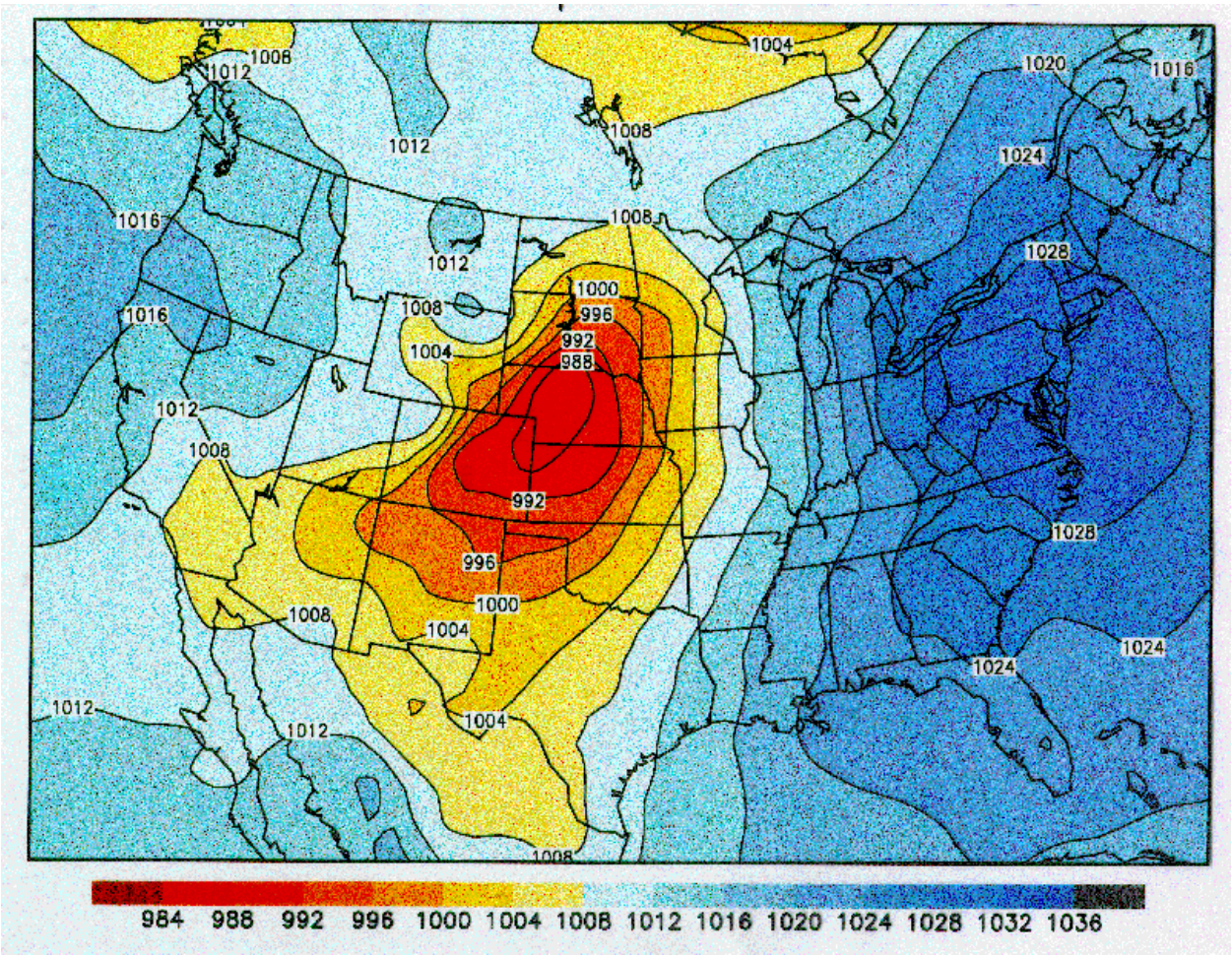

Fig. 3.3 As in Fig. 3.2, but with enhanced gravity wave drag.

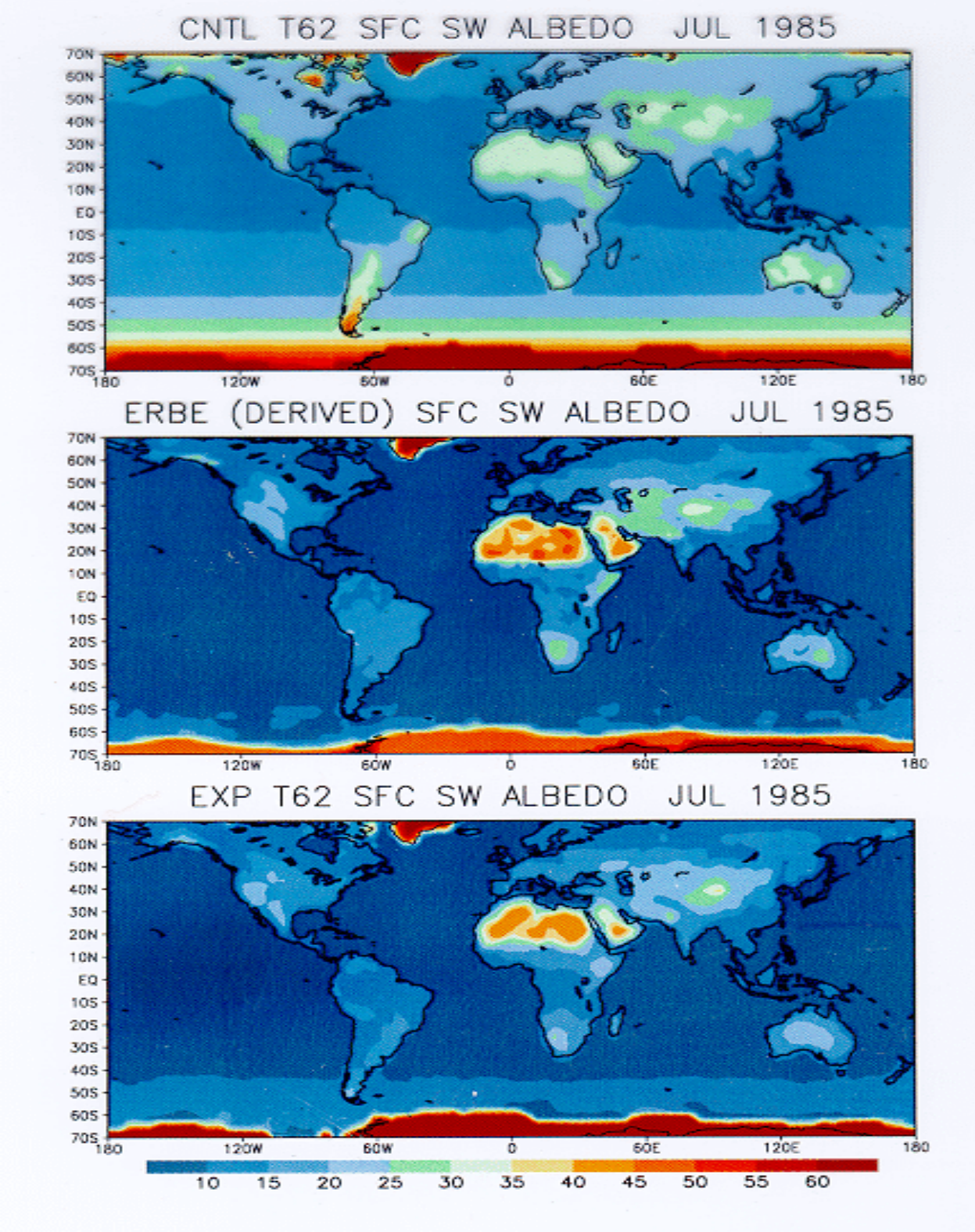

Fig. 3.4 Surface shortwave albedo for July 1985: Operational T62(top), T62 model with new shortwave scheme(bottom) and ERBE-based observations (middle).

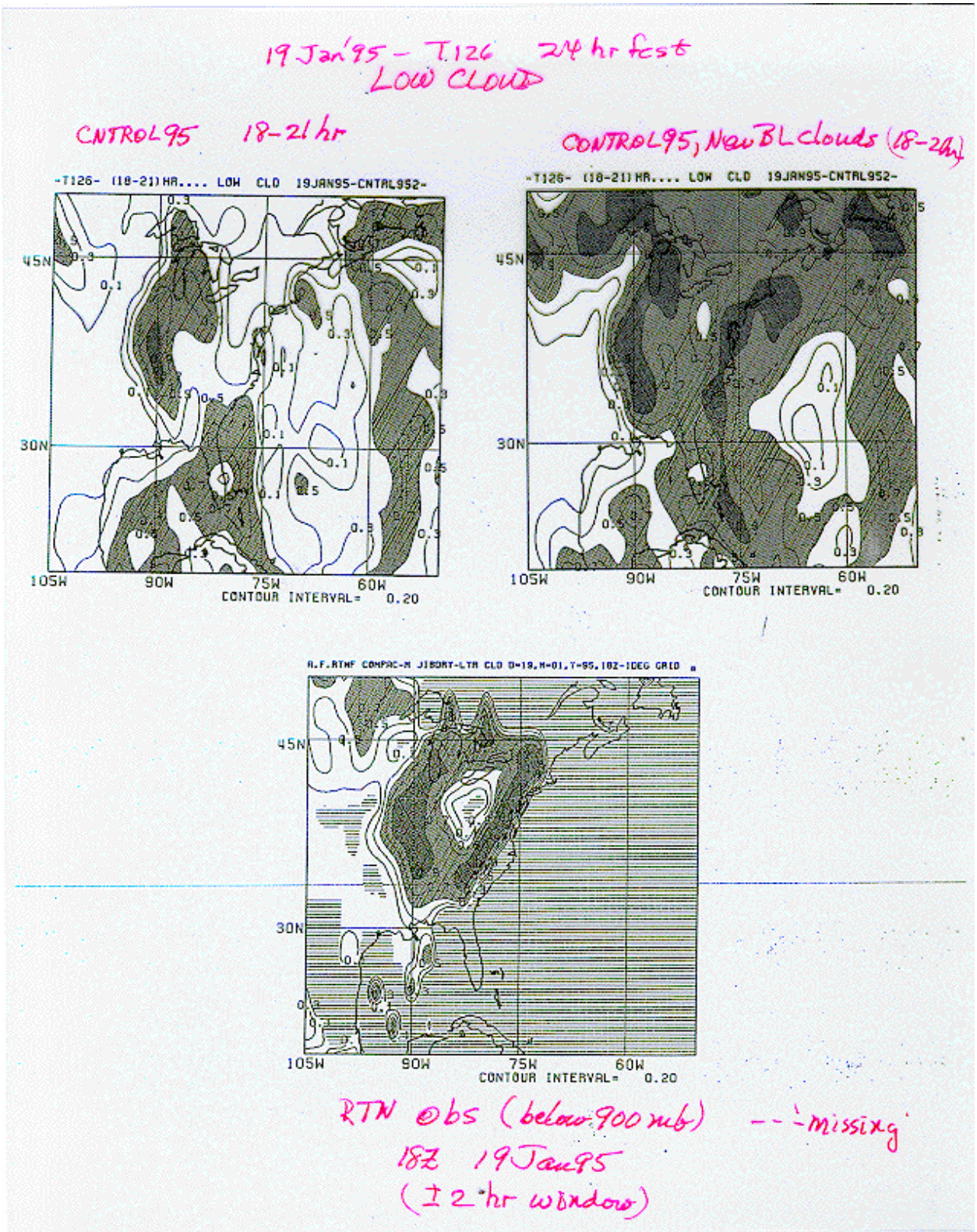

Fig. 3.5 18-21-h forecasts of fractional low cloud cover from the T126L28 operational model (top left), the same model with the new cloud scheme (top right) and RTNEPH data (bottom).

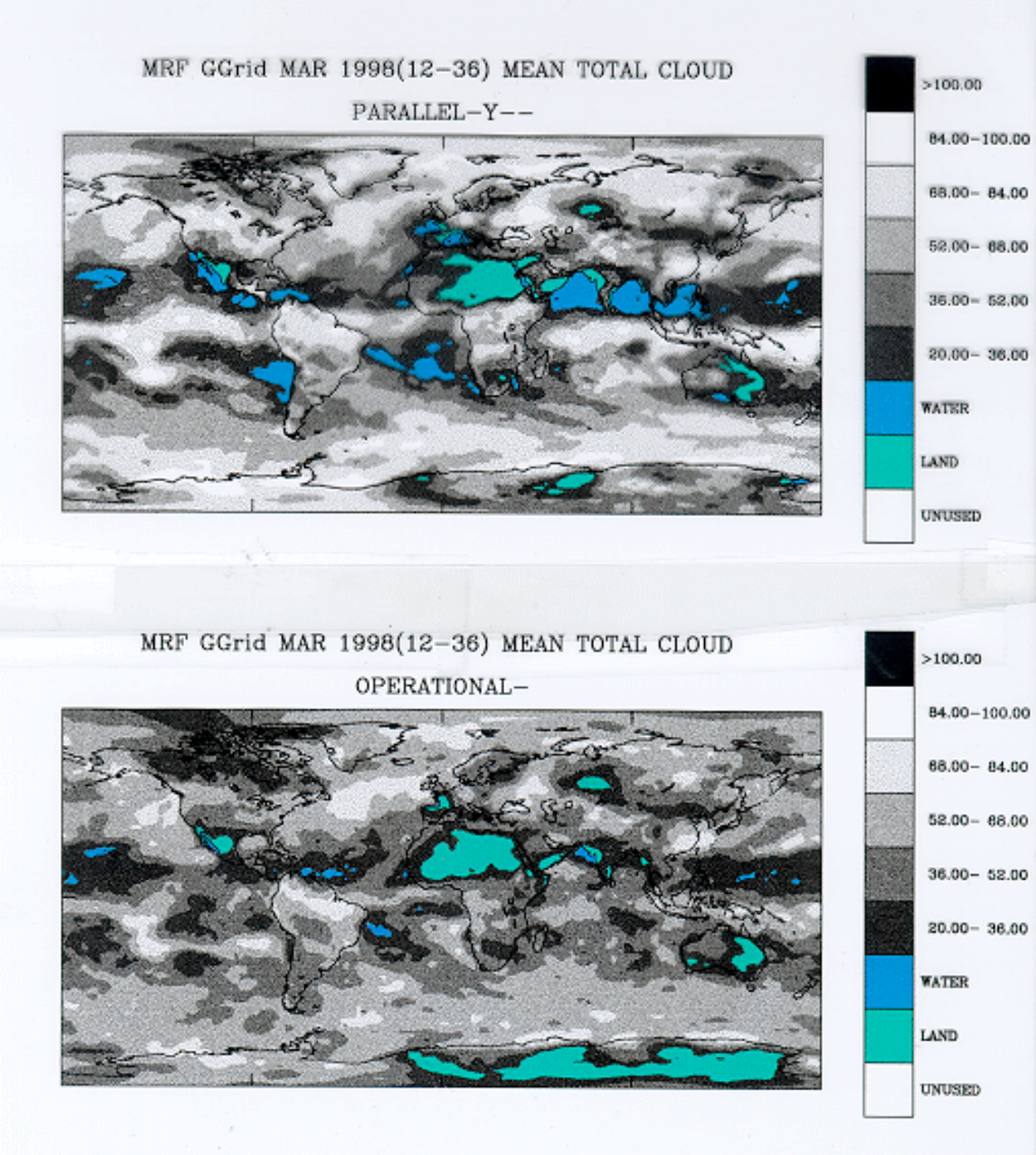

Fig. 3.6 daily mean 12-36 hour total cloud cover forecasts for the period 14-23 March 1998. Top: new model, labeled 'parallel Y'; Middle: operational model; Bottom: RTNEPH observations.

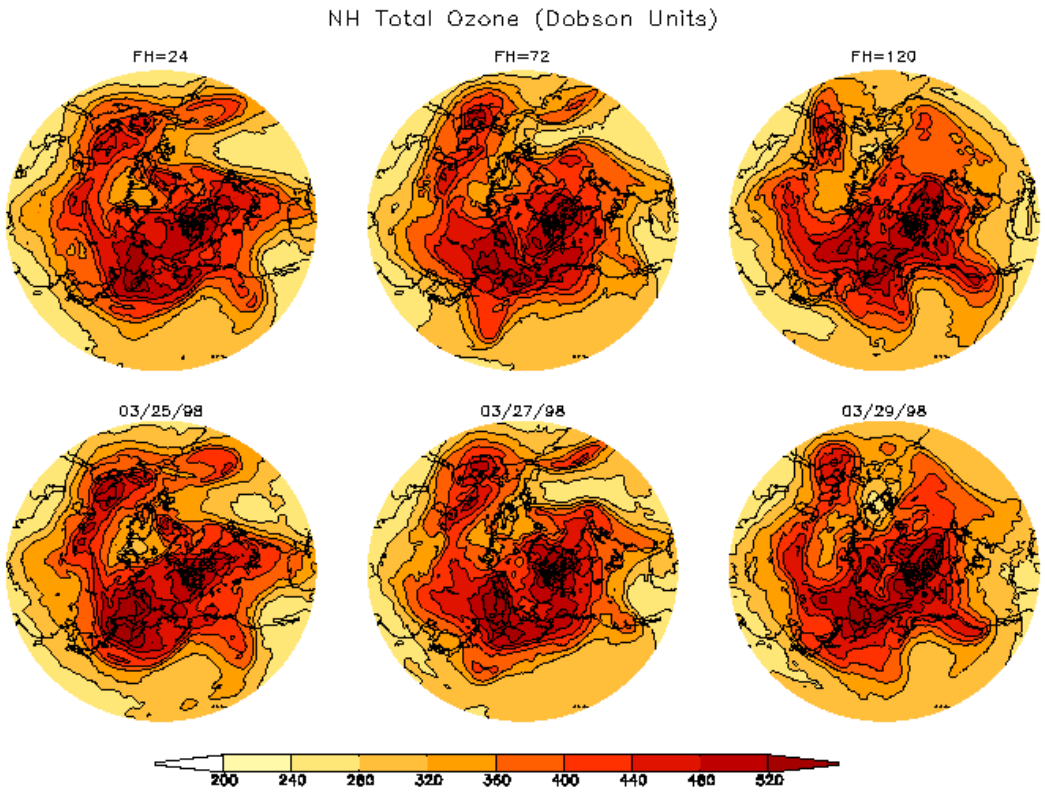

Fig. 3.7a. Total ozone, N. Hemisphere: Forecasts, top row; verifying analyses, bottom row.

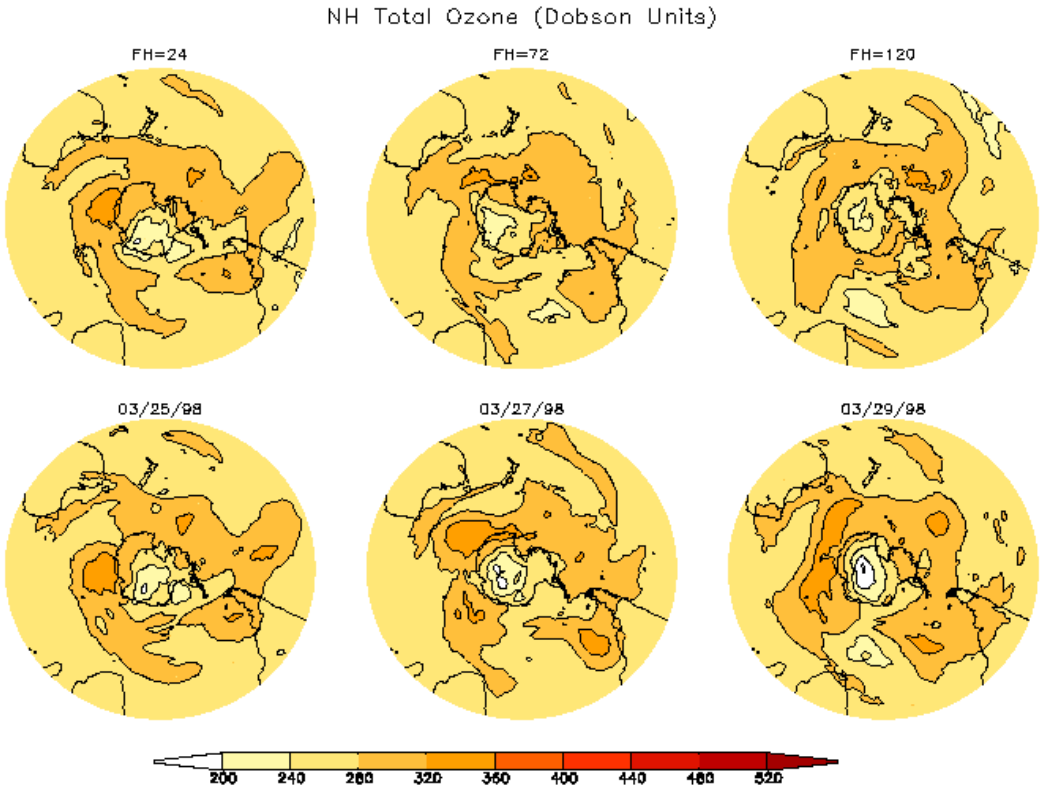

Fig. 3.7b As in Fig. 3.7a, but for S. Hemisphere (label in diagram is wrong).

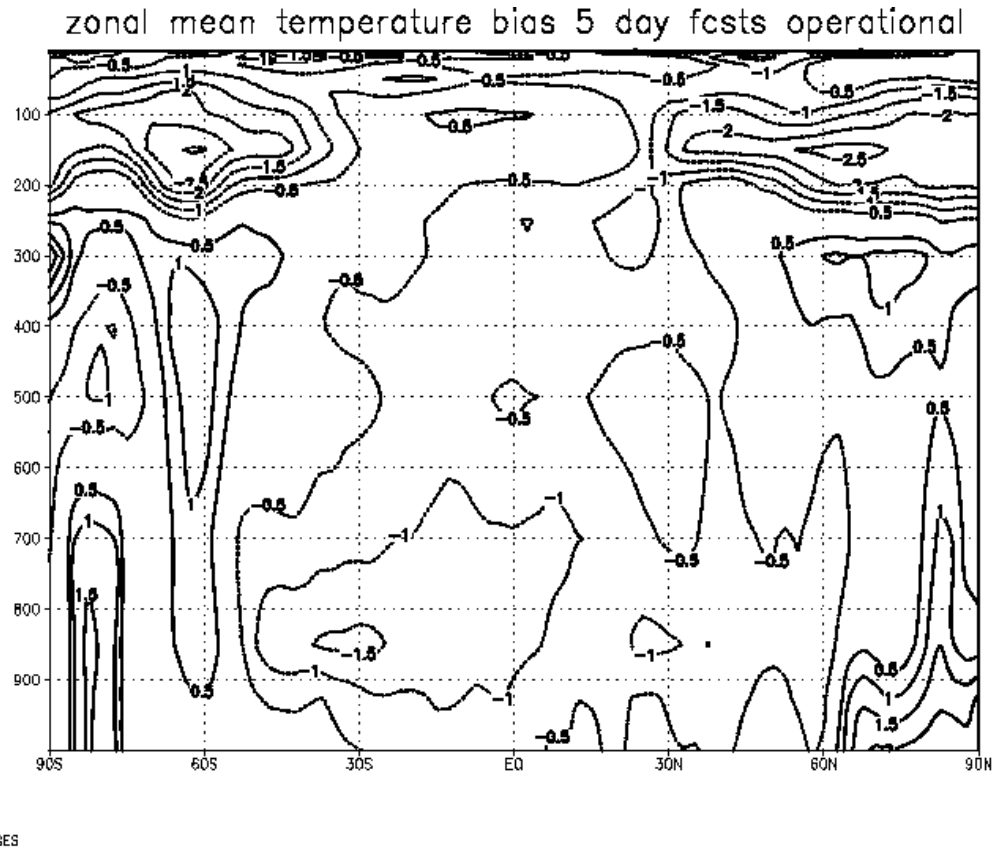

Fig. 5.1 Vertical cross-sections of zonal mean temperature errors for 5-day forecasts averaged over a two-week period for operational system (top) and new system (bottom).

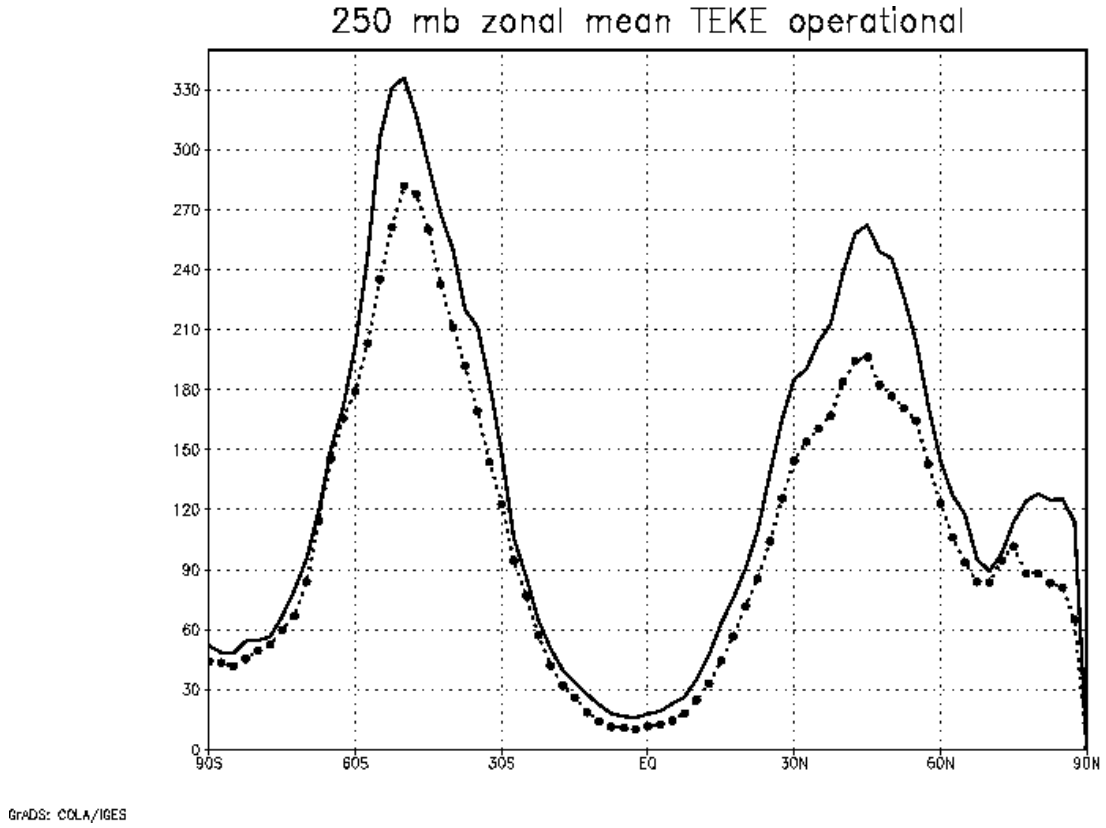

Fig. 5.2a Zonal mean transient eddy kinetic energy at 200 hPa averaged over two weeks of 5-day forecasts (dotted line) compared to verifying analyses (solid line) for operational model. Units are m2/sec2.

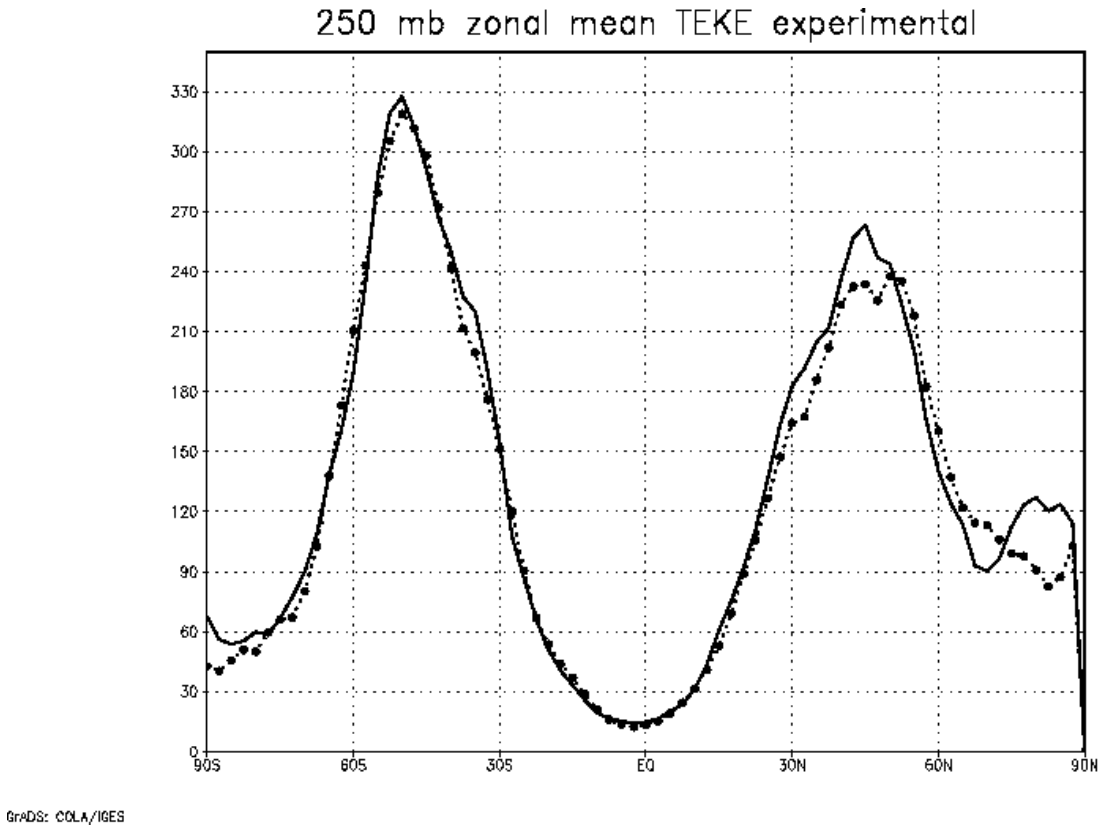

Fig. 5.2b Zonal mean transient eddy kinetic energy at 200 hPa averaged over two weeks of 5-day forecasts (dotted line) compared to verifying analyses (solid line) for operational model. Units are m2/sec2.

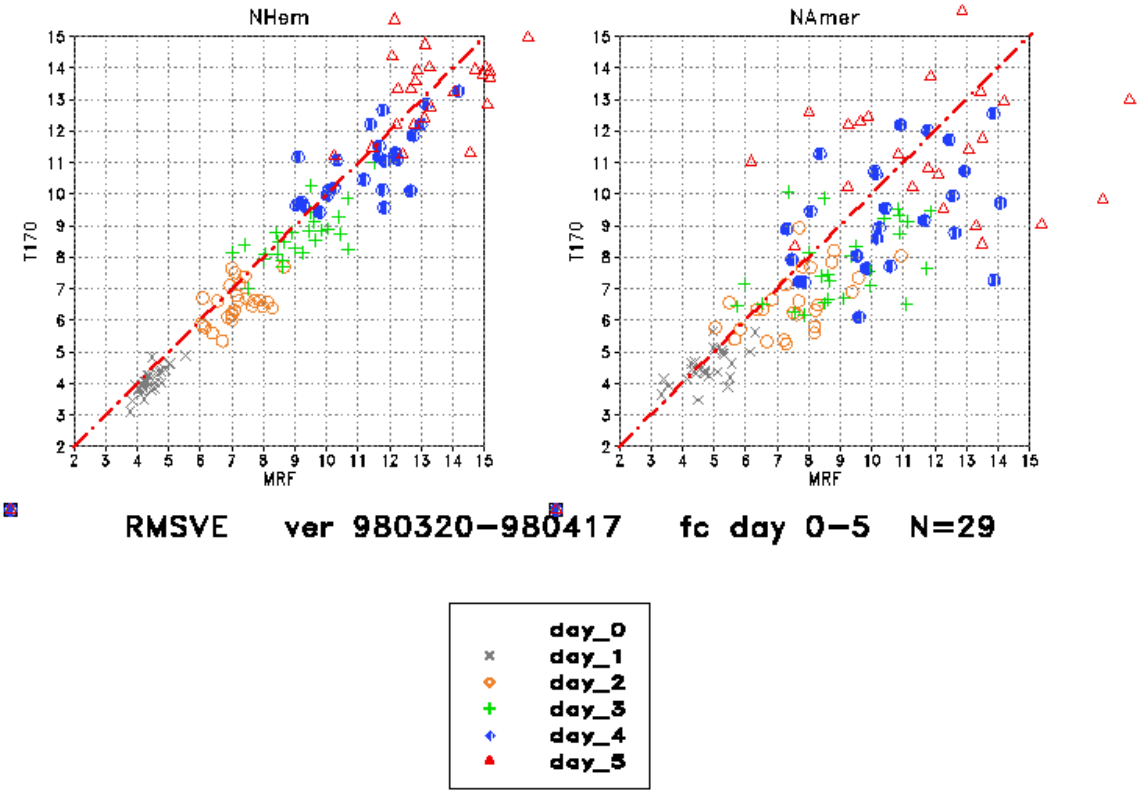

Fig. 5.3 Rms vector wind errors (m/sec) at 200 hPa for operational system (MRF) vs. new system (T170) for forecasts for days 0-5 verifying over a 29-day period, verified over the N. Hemisphere (left) and North America (right). Different forecast lengths are indicated by the various symbols; cases in which the new system was better appear in the lower right part of each plot.

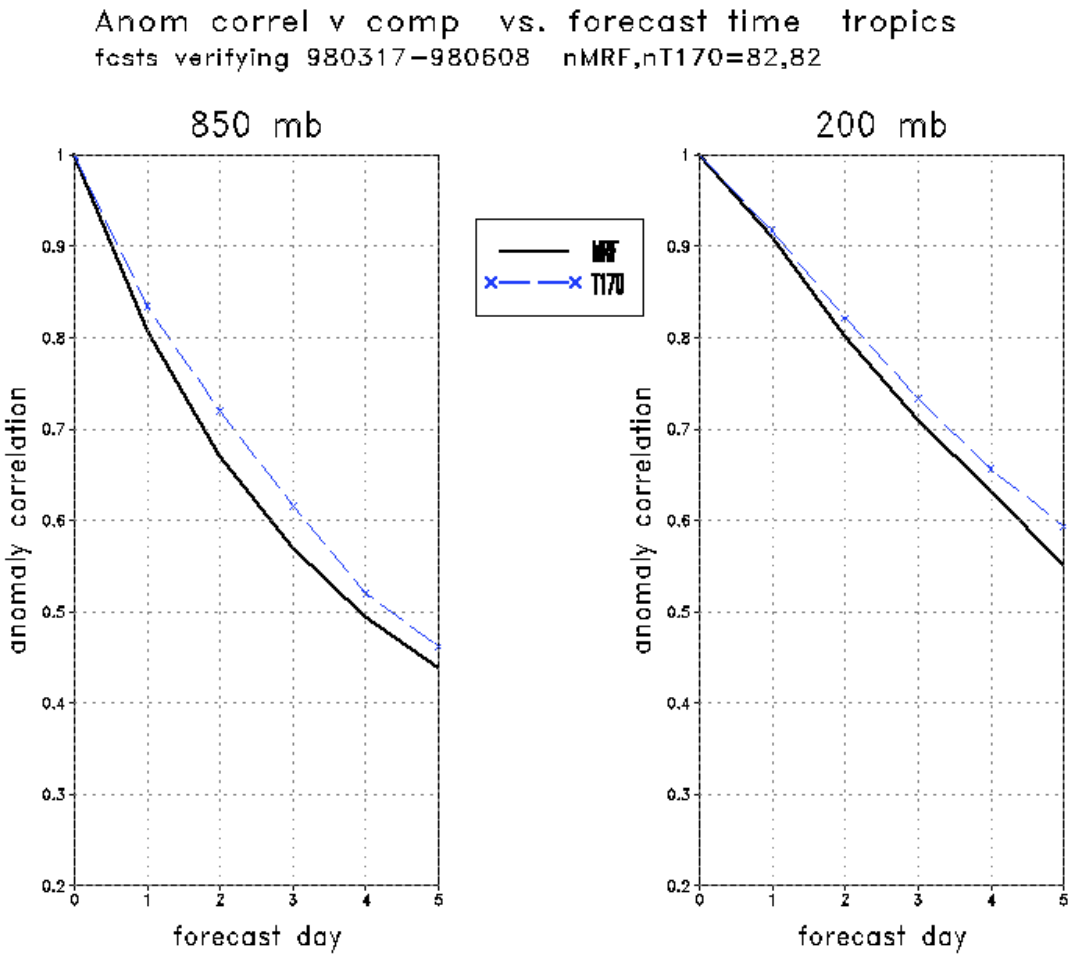

Fig. 5.4 Average of anomaly correlation as a function of forecast length for v-component of wind at the 850-hPa (left) and 200-hPa (right) levels in the tropics (20S-20N) for the operational (MRF), ECMWF (ec) and new (T170) models for 82 cases.

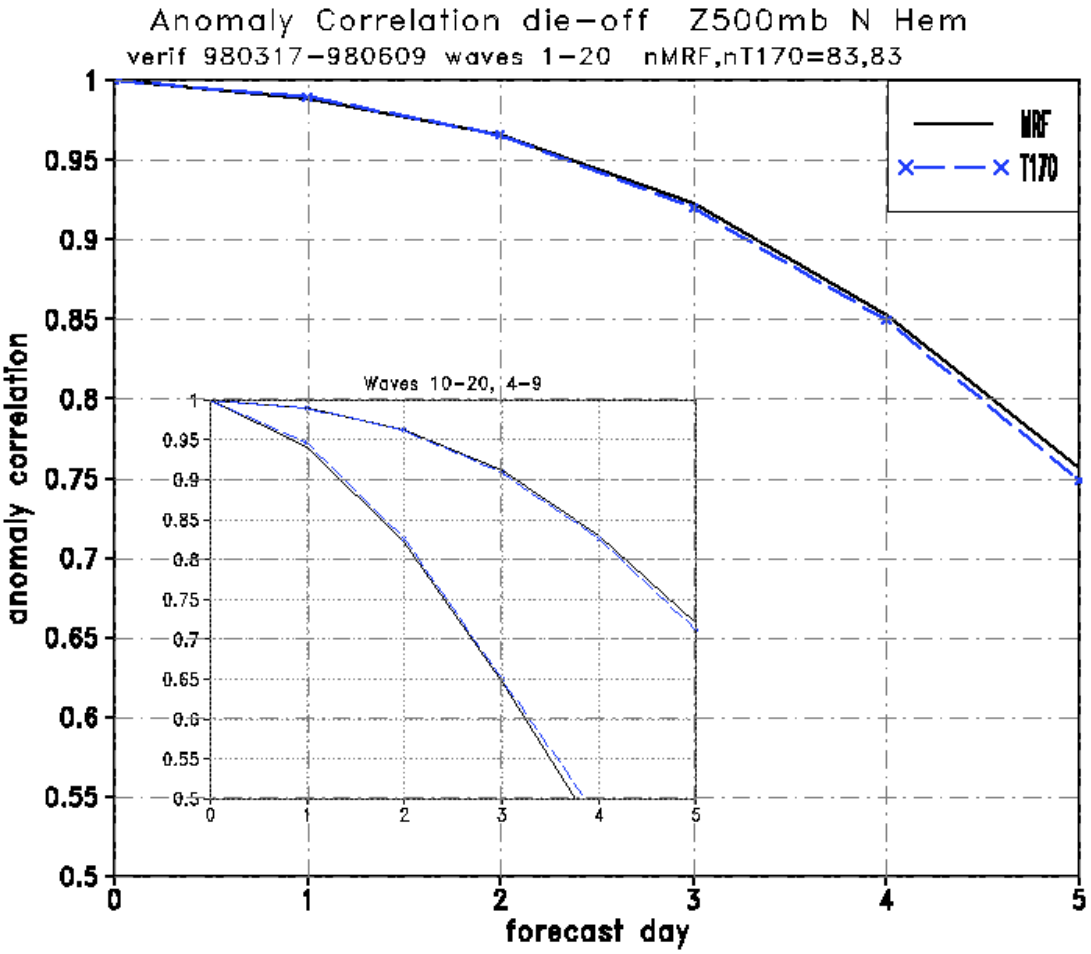

Fig. 5.5 Averaged anomaly correlations for 500-hPa heights as a function of forecast length and zonal wave number group for 83 days of forecasts for the operational system (MRF), the new system (T170) and the ECMWF (ec) for the N. Hemisphere (top) and S. Hemisphere (bottom).

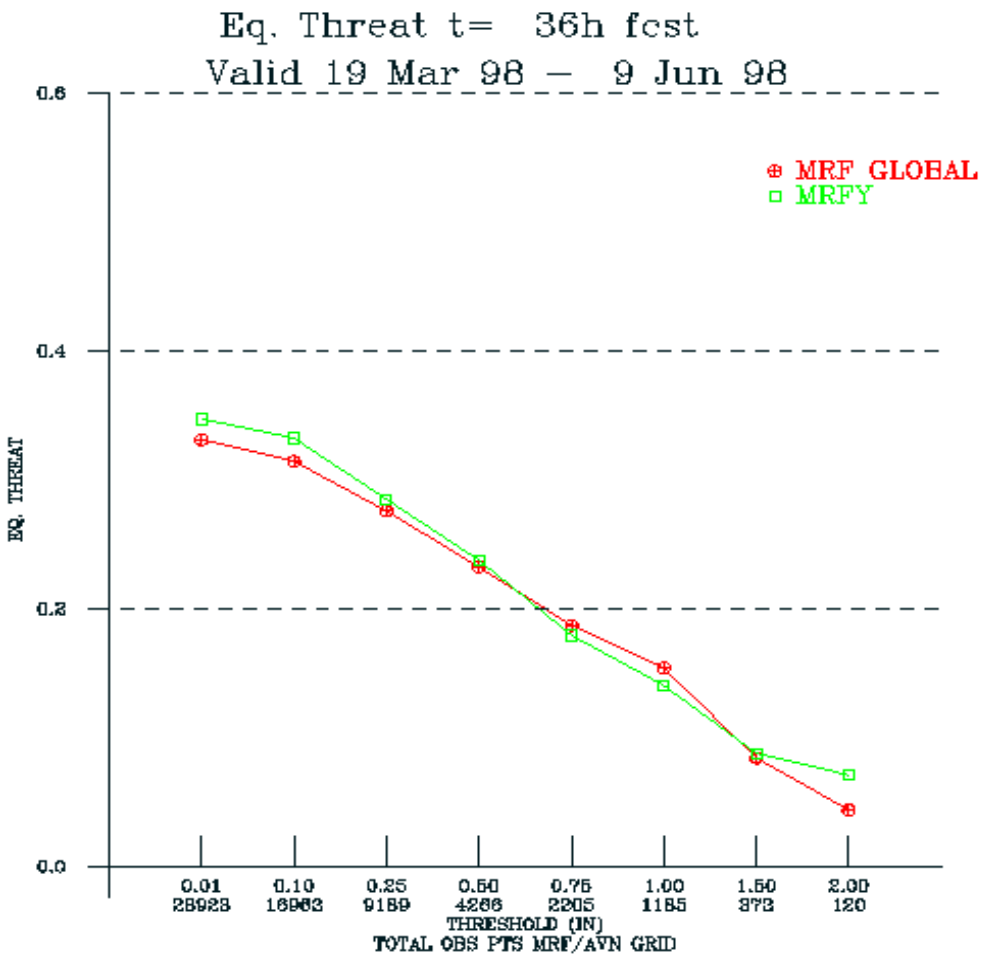

Fig. 5.6a Threat score for 36-h precipitation forecasts valid 19 March - 9 June 1998 as a function of amount for stations in the U.S. Operational system (MRF Global) indicated by circles; new system (MRFY) by squares. Numbers below x-axis indicate number of observations above each precipitation threshold.

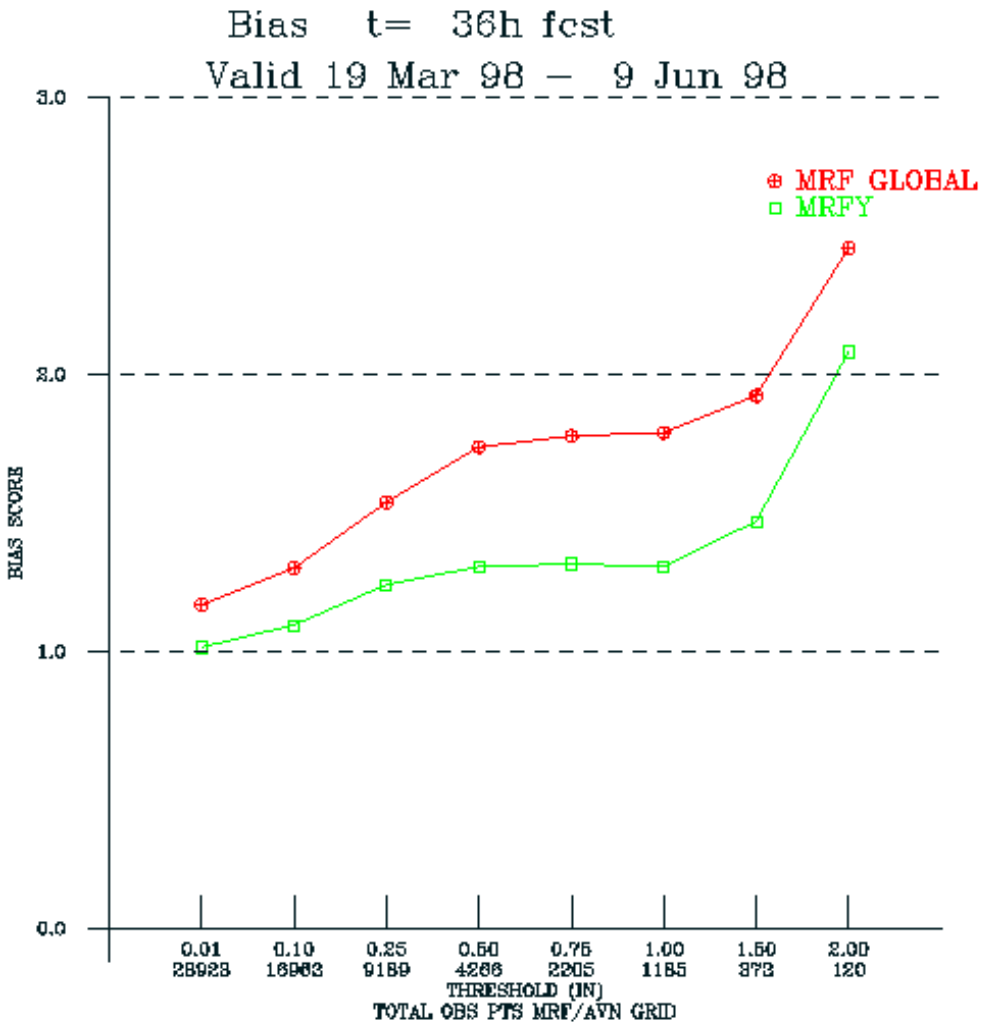

Fig. 5.6b Same as in Fig 5.6a, but for bias.

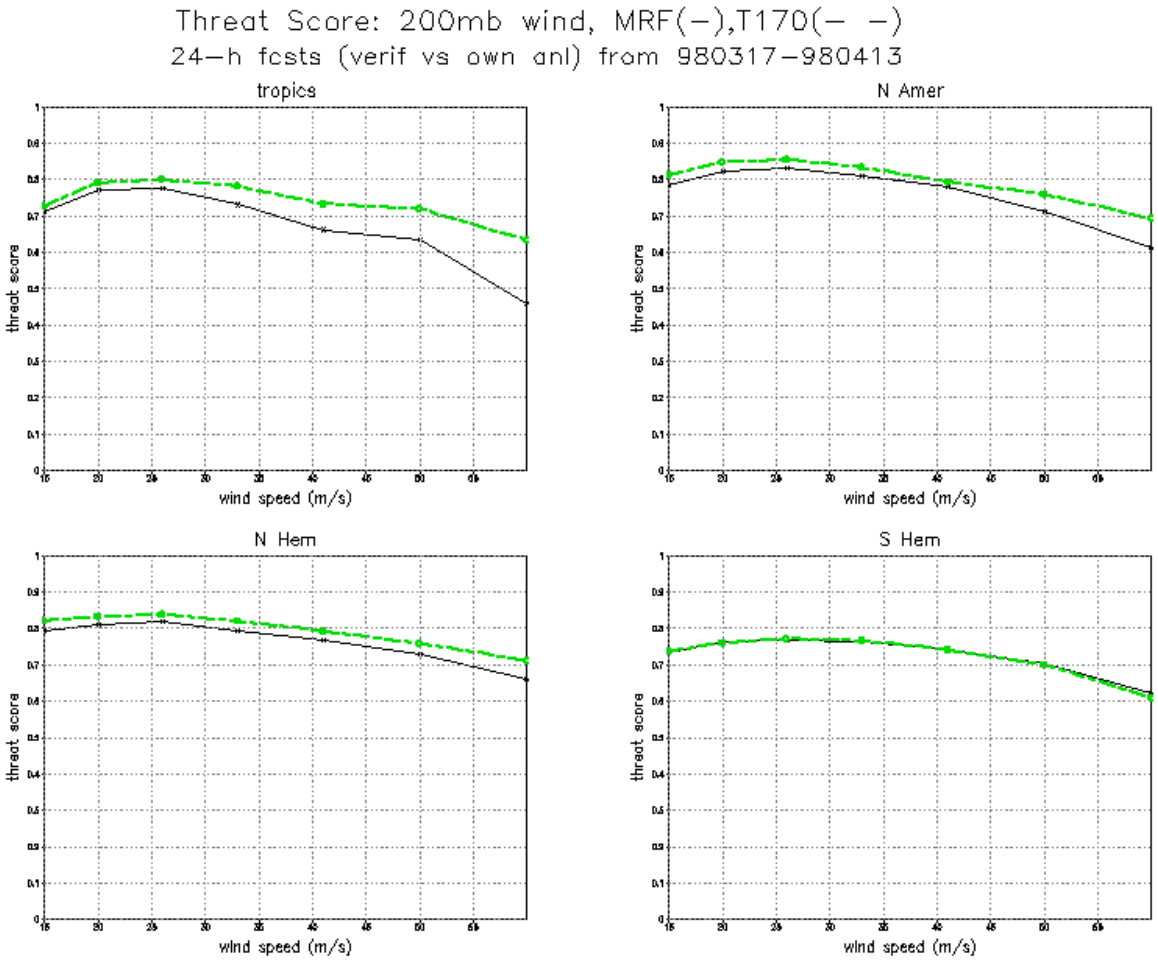

Fig. 5.7a Equitable threat scores for 24-h 200 hPa forecasts of wind speed for four regions for the operational model (MRF, solid) and new model (T170, dashed).

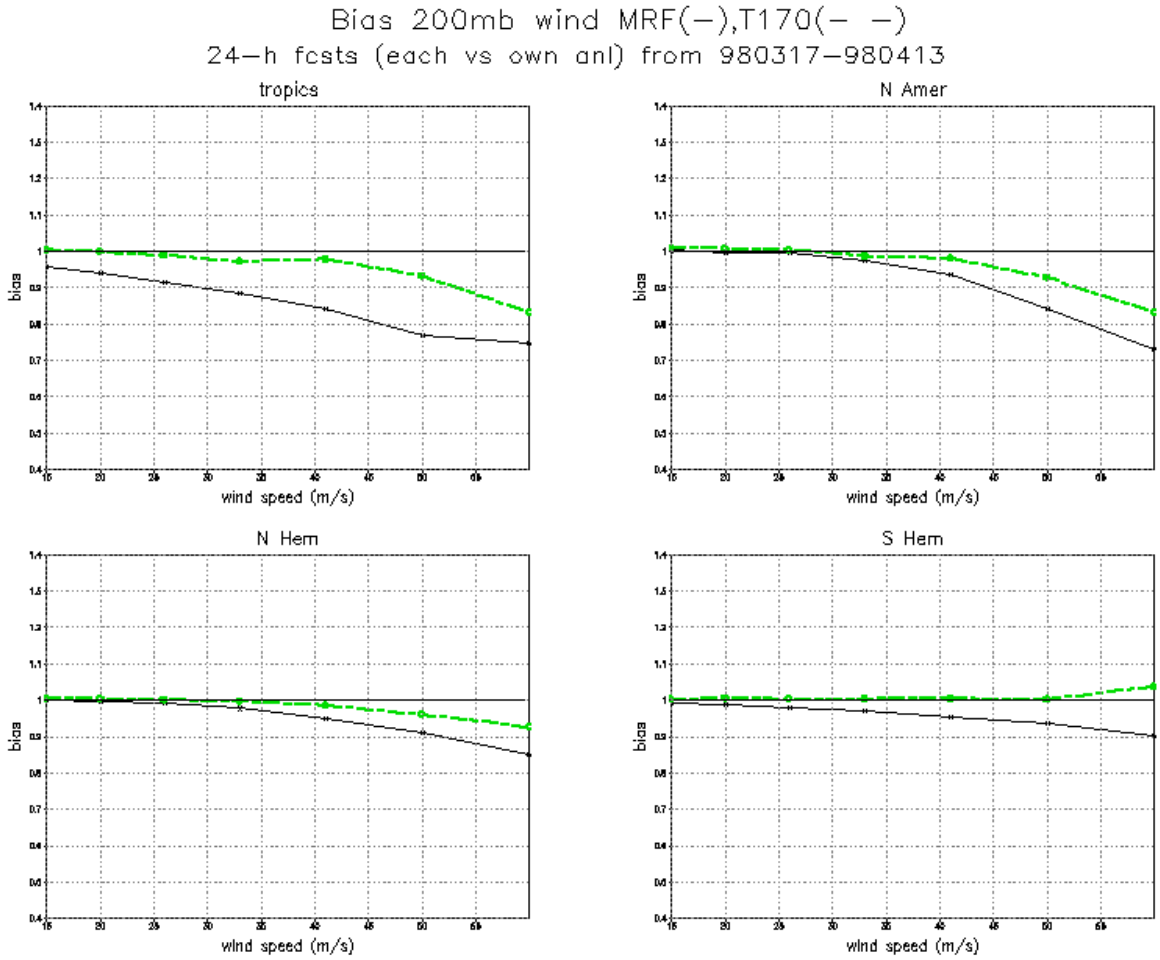

Fig. 5.7b As in Fig 5.7a, but for wind speed bias.

Default configuration of the global model system

Network	Runs per day	Analysis resolution	Forecast hours at T170L42	Forecast hours at T126L28	Forecast hours at T62L28
Final GDAS	4	T170 L42	0-9	---	---
Aviation	4	T170 L42	0-78	---	---
MRF	1	N/A	0-84	84-168	168-384
Ensemble	16	N/A	---	---	0-384

Backup configuration of the global model system

Network	Runs per day	Analysis resolution	Forecast hours at T170L42	Forecast hours at T126L28	Forecast hours at T62L28
Final GDAS	4	T170 L42	0-9	---	---
Aviation	4	T126 L28	---	0-78	---
MRF	1	---	---	0-168	168-384
Ensemble	16	---	---	---	0-384

Table 1 - Configurations of the Modeling System